J Biol Inorg Chem (2005) 10: 417–424
DOI 10.1007/s00775-005-0656-2

ORIGINAL ARTICLE

**Alex H. Priem · Adri A. K. Klaassen
Eduard J. Reijerse · Terrance E. Meyer
Claudio Luchinat · Francesco Capozzi
William R. Dunham · Wilfred R. Hagen**

EPR analysis of multiple forms of $[4Fe-4S]^{3+}$ clusters in HiPIPs

Received: 3 August 2004 / Accepted: 22 April 2005 / Published online: 12 May 2005

Abstract The electron paramagnetic resonance (EPR) spectrum from the $[4Fe–4S]^{3+}$ cluster in several high-potential iron–sulfur proteins (HiPIPs) is complex: it is not the pattern of a single, isolated $S=1/2$ system. Multifrequency EPR from 9 to 130 GHz reveals that the apparent peak positions (g values) are frequency-independent: the spectrum is dominated by the Zeeman interaction plus g-strain broadening. The spectra taken at frequencies above the X-band are increasingly sensitive to rapid-passage effects; therefore, the X-band data, which are slightly additionally broadened by dipolar interaction, were used for quantitative spectral analysis. For a single geometrical $[4Fe–4S]^{3+}$ structure the $(Fe–Fe)^{5+}$ mixed-valence dimer can be assigned in six different ways to a pair of iron ions, and this defines six valence isomers. Systematic multicomponent g-strain simulation shows that the $[4Fe–4S]^{3+}$ paramagnets in seven HiPIPs from different bacteria each consist of three to four discernible species, and these are assigned to valence isomers of the clusters. This interpretation builds on previous EPR analyzes of $[4Fe–4S]^{3+}$ model compounds, and it constitutes a high-resolution extension of the current literature model, proposed from paramagnetic NMR studies.

Keywords High-potential iron–sulfur protein · Exchange · Electron paramagnetic resonance · Mixed valence

A. H. Priem
Department of Molecular Spectroscopy,
University of Nijmegen, The Netherlands

A. A. K. Klaassen
Department of Physical Chemistry
(Solid State NMR Spectroscopy),
University of Nijmegen, The Netherlands

E. J. Reijerse
Max Planck Institute for Bioinorganic Chemistry,
Mülheim, Germany

T. E. Meyer
Department of Biochemistry,
University of Arizona, Tucson, AZ, USA

C. Luchinat
Centro Risonanze Magnetiche—CERM,
University of Florence, Italy

F. Capozzi
Department of Food Science,
University of Bologna, Italy

W. R. Dunham
Biophysics Research Division,
University of Michigan,
Ann Arbor, MI, USA

W. R. Hagen (✉)
Department of Biotechnology,
Delft University of Technology,
Julianalaan 67, 2628 BC Delft, The Netherlands
E-mail: w.r.hagen@tnw.tudelft.nl
Tel.: +31-15-2785051
Fax: +31-15-2782355

Introduction

The paramagnetic metal ions in biological and synthetic iron–sulfur clusters interact through the bonds of their bridging sulfur atoms and possibly also directly through space, and this results in an integral electronic structure with associated cluster magnetism. Magnetic spectroscopies are used extensively to monitor iron–sulfur clusters as a function of their biological structure and mechanism of action; however, cluster magnetism is complex and only partially understood, especially for the larger clusters.

For the paramagnetism of the reduced dinuclear cluster $[2Fe–2S]^{1+}$ in proteins the dominant interaction is strong antiferromagnetic superexchange coupling between the irons. This results in spin ladders with low-spin ground states observed in electron paramagnetic resonance (EPR) spectroscopy, exchange-induced paramagnetic shifts in NMR, and localized valence, i.e., cluster reduction leads to an

extra electron localized on a specific iron ion (summarized in Ref. [1]). The paramagnetic NMR shifts have subsequently been related to the localized valencies of the irons (summarized in Ref. [2]).

Extending the analysis to larger clusters has been found to be nontrivial because there is also the double-exchange interaction associated with a delocalization of the extra charges from reduction over more than one iron [3]. The [4Fe–4S] cores are commonly envisioned as made up of iron pairs dominated by double exchange. For example, the $[4Fe–4S]^{3+}$ core in high-potential iron–sulfur proteins (HiPIPs) can be thought of as the combination of a ferric pair (Fe^{3+}–Fe^{3+}) and a mixed-valence pair ($Fe^{2.5+}$–$Fe^{2.5+}$). This model has been used to explain signs of ^{57}Fe hyperfine couplings observed in low-temperature Mössbauer spectra [4–6].

Theoretically, there are six different ways to take two Fe ions in a [4Fe–4S] cluster to form a mixed-valence pair: there are six valence isomers. Since the surrounding of the cluster in the proteins is asymmetric, the six possibilities should be electronically inequivalent and therefore distinguishable. Paramagnetic shifts in ^{1}H-NMR data of oxidized HiPIPs provide a clear indication for the occurrence at room temperature of more than one valence isomer. The NMR experiment defines a fast-exchange situation, and it has therefore been interpreted in terms of the average of (at least) two valence isomers [2, 7, 8].

Multiple signals of $[4Fe–4S]^{3+}$ sites have been observed in the low-temperature EPR of γ-irradiated single crystals of synthetic model compounds [9, 10]. Apparent multiplicity has also been found in the EPR of HiPIPs [11, 12]; however, spectral data analysis has been based on ad hoc models for EPR spectral shapes, which lack theoretical foundation [13–15]. We have systematically reinvestigated the magnetic structure of HiPIP $[4Fe–4S]^{3+}$ clusters using multifrequency EPR spectroscopy and quantitative *g*-strain analysis.

Materials and methods

Proteins

The HiPIPs used in this study were from *Ectothiorhodospira vacuolata* DSM 2111, ATCC 43036 (heterotypic synonym *E. shaposhnicovii*) isoprotein I and isoprotein II, *Rhodopila globiformis* DSM 161, ATCC 35887 (basonym *R. globiformis*), *Rubrivivax gelatinosus* DSM 1709, ATCC 17011 (basonym *Rhodocyclus gelatinosus*, also basonym *Rhodopseudomonas gelatinosa*), *Rhodocyclus tenuis* DSM 109, ATCC 25093 (basonym *Rhodospirillum tenue*), *Allochromatium vinosum* DSM 180, ATCC 17899 (basonym *Chromatium vinosum*), and *Halorhodospira halophila* DSM 244 (basonym *E. halophila*) isoprotein I. The purification procedures were cited in Ref. [16], except that for *E. halophila* [8].

Spectroscopy

The X-band (9 GHz) EPR was done with a Bruker ER 200 spectrometer. The Q-band (35 GHz) spectrometer was constructed from a Varian E 110 Q-band bridge, a Varian 60 MHz NMR magnet connected to a Varian EPR power supply, a PAR 117 lock-in amplifier and a homebuilt cryo-insert plus modulation unit. The high-Q cylindrical TE011 cavity was constructed from silver-plated "wonderstone" ceramic (pyrophyllite). The D-band (130 GHz) spectrometer was described previously in Ref. [17].

Results and discussion

Definition of the basic cluster model

The oxidized cubane cluster in HiPIPs $[4Fe–4S]^{3+}$ formally contains three Fe^{III} ferric ions and one Fe^{II} ferrous ion. Each iron ion is in a distorted tetrahedral ligand field of three acid-labile μ_3-S^{2-} sulfides and one thiolato S^{2-} from cysteine. Mössbauer spectroscopy showed that all four irons form an integrated electronic system that behaves as a single paramagnet with a ground-state system spin $S = 1/2$ [4, 6, 18]. This spin is thought to be the result of pairwise electronic exchange interactions between iron ion pairs [4], where each pair is envisioned as the net result of two opposing interactions, namely, of superexchange, via the bridging sulfides, favoring antiparallel coupling of individual ion spins, and of double-exchange, associated with electron delocalization over the pair, favoring parallel spin coupling [2, 3, 5]. The system spin can be constructed from the individual spins, $S = 5/2$ from Fe^{III} and $S = 2$ from Fe^{II}, in a stepwise combinatorial procedure with pairs of iron ions as intermediate building blocks. Thus, two Fe^{III} ions can be combined into a ferric pair with a combination spin $S_{pair} = 5/2 + 5/2 = 5$ if double exchange dominates, or $S_{pair} = 5/2–5/2 = 0$ if superexchange dominates, or an intermediate value of $0 < S_{pair} < 5$ if the two interactions are comparable in strength. Similarly, the remaining Fe^{III} and Fe^{II} ions can be combined in a mixed-valence pair with a combination spin $1/2 \le S_{pair} \le 9/2$. This description is called the pair-of-pairs model; ligation by an asymmetric protein affords six inequivalent valence isomers.

The EPR model: restricted *g* strain

EPR spectroscopy, as a direct monitor of valence electrons, might be expected to be particularly suitable for the detection of valence isomer configurations. However, a key difficulty is the proper description of the shape of the inhomogeneously broadened EPR line and of the angular dependency of the associated line width. The statistical *g*-strain model [15–17], which is founded in

Table 1 Parameters of different electron paramagnetic resonance simulation models for *Allochromatium vinosum* high-potential iron–sulfur protein (*HiPIP*)

Intensity	g_z, g_y, g_x	Δ_z, Δ_y, $\Delta_x \times 10^{-3}$
Model a (single axial component)		
1	2.126, 2.042, 2.042	9, 9, 9
Model b (single rhombic component)		
1	2.126, 2.0485, 2.035	8, 9, 6
Model c (all remaining features are one rhombic component)		
0.95	2.126, 2.0485, 2.035	8, 9, 6
0.05	2.147, 2.09, 2.06	7, 5, 3
Model d (remaining features are absorption-like)		
0.76	2.126, 2.0485, 2.035	8, 9, 6
0.12	2.145, 2.04, 2.04	8, 8, 8
0.12	2.090, 2.04, 2.04	8, 8, 8
Model e (all minor features are g_z from rhombic spectra)		
0.68	2.126, 2.0485, 2.035	8, 9, 6
0.12	2.109, 2.05, 2.04	8, 9, 5
0.12	2.090, 2.05, 2.04	8, 9, 5
0.08	2.145, 2.05, 2.04	8, 9, 5

Table 2 *g*-strain parameters and weighing factors for selected HiPIPs

Fraction	g_z, g_y, g_x	Δ_z, Δ_y, $\Delta_x \times 10^{-3}$
Halorhodospira halophila isoprotein I		
0.91	2.1435, 2.035, 2.0295	12.5, 8.8, 9
0.05	2.11, 2.04, 2.03	12.5, 8.8, 9
0.04	2.08, 2.04, 2.03	12.5, 8.8, 9
Rhodopila globiformis		
0.80	2.128, 2.039, 2.025	12.5, 10, 9
0.12	2.10, 2.03, 2.03	11, 9, 9
0.08	2.08, 2.03, 2.03	11, 9, 9
Ectothiorhodospira vacuolata isoprotein I		
0.70	2.109, 2.0287, 2.0287	10, 10.5, 10.5
0.14	2.0438, 2.03, 2.01	2.5, 4, 5
0.08	2.138, 2.03, 2.03	9, 9, 9
0.08	2.077, 2.03, 2.03	9, 8.5, 8.5
E. vacuolata isoprotein II		
0.70	2.112, 2.038, 2.025	8, 6.5, 6.5
0.13	2.135, 2.03, 2.03	9, 6.5, 6.5
0.10	2.095, 2.03, 2.03	8, 6.5, 6.5
0.07	2.075, 2.03, 2.03	8, 6.5, 6.5
Rubrivivax gelatinosus		
0.64	2.1127, 2.0305, 2.0305	7.5, 7.5, 7.5
0.13	2.094, 2.03, 2.03	8.5, 7, 7
0.13	2.076, 2.03, 2.03	8.5, 7, 7
0.10	2.047, 2.00, 1.98	8, 8, 8
Rhodocyclus tenuis		
0.67	2.110, 2.0388, 2.024	7.5, 5.5, 5
0.20	2.095, 2.04, 2.02	9, 5.5, 5
0.13	2.075, 2.04, 2.02	8, 5.5, 5

extensive theoretical and experimental studies in the 1970s and 1980s mainly with reference to EPR spectra of Fe/S proteins, predicts a near Gaussian distribution of g values as a result of microheterogeneity, with an angular dependence of the distribution width described by a symmetrical line-width tensor that is not collinear with the g matrix. In practical terms this means that each independent spectral $S = 1/2$ component is described by (minimally) ten parameters: a relative concentration, three g values, and six g-strain line-width parameters. For a one $[4Fe–4S]^{3+}$ cluster containing protein in a single conformation subject to sixfold valence isomerism the g-strain model would require (minimally) 60 independent parameters to be fit.

Obviously, such an analysis could not be meaningfully applied to a HiPIP EPR spectrum, whose shape (see later) is typically that of a near-axial powder pattern plus minor additional peaks in between the main g_z and g_{xy} features. In order to keep the problem tractable we propose to use a reduced g-strain model that is suitably simplified for application to HiPIP spectra on two counts:

1. Line-width matrices are initially assumed to be diagonal. This reduces the number of parameters per spectral component by 3. The reduction (initially) eliminates the possibility to simulate spectral asymmetries such as peak skewings. Some justification for this simplification may be found in the observation that HiPIP spectra are nearly axial. The shape of axial spectra appears to be relatively insensitive to nondiagonal g strain [19].
2. Spectral multiplicity in HiPIP EPR spectra is mainly apparent in the low-field part, the g_z area. One must, therefore, concede from the onset of the analysis that the spectral resolution in the high-field part, the g_{xy} area, will be limited in the sense that the fitted g_{xy} area will be predominantly determined by the main valence isomer of the highest concentration, and that for all further isomer contributions added to the overall fit, the perpendicular fit parameters (g_x, g_y, Δ_{xx}, Δ_{yy}, see later) are essentially *dummy* fit parameters.

The actual procedure was as follows. The experimental spectrum was simulated with an increasing number of $S = 1/2$ spectral components with diagonal g-strain matrices. In a last optimization round off-diagonal g-strain matrix elements were also fit. The final simulation data, as reported in Tables 1 and 2, were obtained by eliminating all data and/or digits considered to be insignificant, namely, (1) all off-diagonal line-width data, (2) the fourth and higher digit of g_x and g_y from all but the most intense component, and (3) all spectral components with intensities less than 5% of that of the most intense component. Inclusion of these data would cause a barely detectable improvement of the fit, which was, however, considered insignificant because other parameter settings resulted in similar slight improvements, i.e., these minor improvements were not uniquely determined.

Multifrequency EPR of HiPIPs

The EPR of $[2Fe–2S]^{1+}$ in proteins is determined by a combination of interactions independent of the external

field, ***B***, and interactions linear in ***B*** (Zeeman interaction and *g*-strain). Increasing the microwave frequency and, therefore, the field ***B*** makes the interactions linear in ***B*** dominant [20], which is a condition to determine the multiplicity (if any) and stoichiometry of individual components corresponding to the spectrum. The situation for $[4Fe–4S]^{3+}$ clusters in HiPIPs is less clear. Not many data taken at frequencies other than the X-band have been published [11]. Also, X-band EPR of HiPIPs typically shows a complexity (see later) not found in the spectra of [2Fe–2S] ferredoxins. In one case, *A. vinosum* HiPIP in the presence of 0.2 M NaCl, the complexity has been analyzed in terms of a dipolar interaction resulting from dimerization [18].

We measured the EPR of HiPIPs at 9, 35, and 130 GHz in order to determine the relative contributions of interactions linear in the magnetic field ***B*** and independent of ***B***. As an example, we present in Fig. 1 the multifrequency data for *A. vinosum* HiPIP under nondimerizing conditions. This example was chosen because the *A. vinosum* protein has the most complex spectrum of all HiPIPs studied (see later). The figure shows an unexpected practical difficulty in these types of experiments. Although the samples used were pure and of high concentration (typically several millimolar), and although the EPR spectra are relatively sharp, the Q-band and especially the D-band spectra suffer from relatively poor signal-to-noise ratios and imperfect baselines. We found that the EPR of these systems can only be obtained over a narrow temperature window. This window shifts to higher T values and reduces in width with increasing frequency. Typical limiting values are approximately 15–30 K in the X-band, 25–35 K the in Q-band, and a few degrees around 35 K in the D-band. Above the higher limit, the spectra broaden by lifetime broadening (T_1—or spin–lattice relaxation). Below the lower limit, the spectra progressively distort by rapid-passage effects and eventually become undetectable. In the D-band, it was usually not possible to obtain conventional absorption-derivative spectra. The D-band trace of Fig. 1 was initially obtained in dispersion mode, and subsequently filtered and differentiated according to the method in Ref. [21].

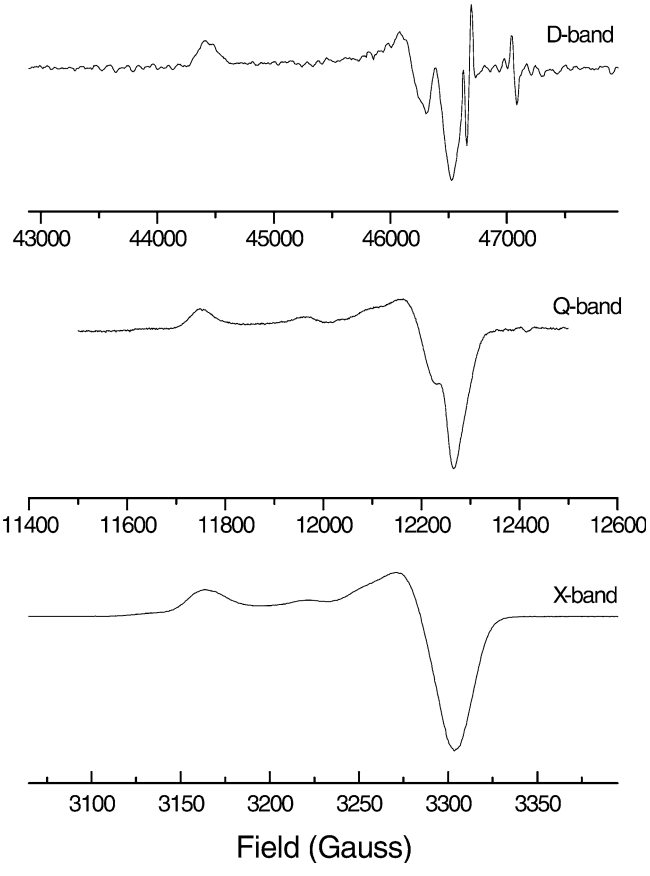

Fig. 1 Multifrequency electron paramagnetic resonance (*EPR*) of *Allochromatium vinosum* high-potential iron–sulfur protein (*HiPIP*) at 130, 35, and 9 GHz. The three spectra were aligned on a reciprocal *g*-value scale to show that all spectral features (except line widths) are positionally invariant, and therefore represent real *g*-values. Two high-field spikes in the D-band spectrum are from cavity contaminants. The EPR conditions (D, Q, and X) were as follows: microwave frequency, 129,987, 34,940, and 9,414 MHz; microwave power, 0.64, 0.5, and 0.2 mW; modulation frequency, 25, 80, and 100 kHz; modulation amplitude, 6, 4, and 4 G; temperature, 35, 25, and 15 K

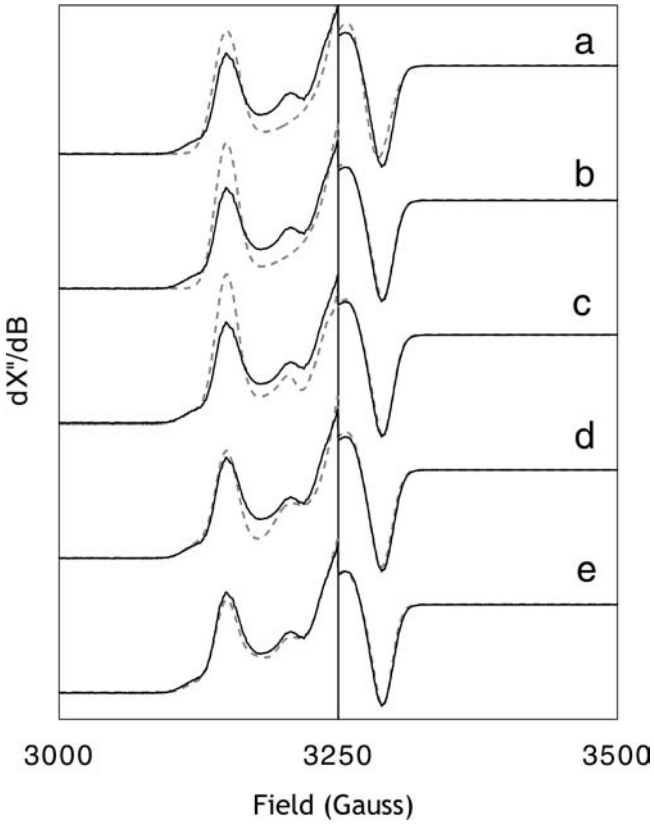

Fig. 2 Different simulation models for the X-band EPR of *A. vinosum* HiPIP. The fitting, with increased complexity, shows that the spectrum consists of (at least) four different components, and these are putatively identified with valence isomers. See the text for details. The fitting parameters for models a–e are given in Table 1

In spite of these unavoidable experimental difficulties, it is clear from Fig. 1 that the *positions* of all the spectral features are invariant in g space; therefore, they are real g values and are not caused by field-independent interactions such as dipole–dipole interactions between clusters in different molecules. This means that one can use the spectra as a basis for multicomponent analysis to identify multiple valence isomers. The X-band spectra are significantly broader than the higher-frequency spectra, which indicates significant contributions of unresolved ***B***-independent interactions. However, we chose to use the X-band data for our component analyzes because (1) the high-frequency data usually suffer from some distortion from rapid-passage effects, which precludes determination of stoichiometries, and (2) the extra broadening at the X-band is not dominant (no spectral feature is lost) and is essentially isotropic; therefore, it can be easily modeled in the numerical analysis with the single global parameter of residual broadening.

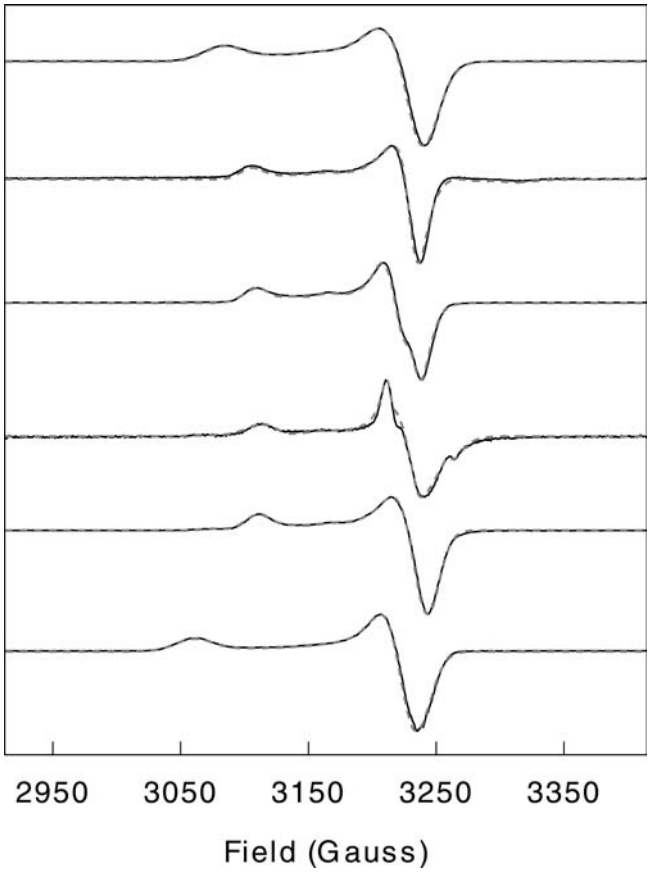

Fig. 3 Optimized simulations of the X-band EPR spectra of HiPIP from (from *top* to *bottom*) *Rhodopila globiformis*, *Rubrivivax gelatinosus*, *Rhodocyclus tenuis*, *Ectothiorhodospira vacuolata* isoprotein I, *E. vacuolata* isoprotein II, and *Halorhodospira halophila* isoprotein I. The fitting parameters are compiled in Table 2. The EPR conditions were as follows: microwave frequency, 9.18 GHz; microwave power, 0.2–0.8 mW; modulation frequency, 100 kHz; modulation amplitude, 5 G; temperature 27 K

Stepwise g-strain analysis of *A. vinosum* wild-type HiPIP

The X-band EPR spectrum of *A. vinosum* HiPIP was analyzed under a g-strain model, starting from the simplest possible assumption of a single component of high symmetry, and subsequently stepwise increasing the complexity of the model until a quantitative fit of the data was obtained. That fit provides the minimum hypothesis for the interpretation of the spectrum. The major conclusion is that the experimental spectrum is consistent with the existence of more than two valence isomers.

The procedure is illustrated in Fig. 2 and the fitting parameters are compiled in Table 1. In the top trace, the experimental spectrum was fitted assuming a single component of axial symmetry (i.e., $g_x = g_y$). This initial fit indicates that there is one major component contributing to the overall spectrum, but that it is not of high symmetry. The next step, trace b, is a fit with a single rhombic spectrum with anisotropic g strain. After optimization, at least three spectral features remain to be accounted for. Also the major "perpendicular" feature (the g_x g_y region) shows a poor fit in terms of the ratio of the positive and negative amplitudes, i.e., the intensity above and below the baseline. Allowing the g strain to be noncolilnear with g (i.e., $\Delta_{ij} \neq 0$) gives no significant improvement (not shown). The smallest step of increasing complexity is to assume that the remaining three features are all from one additional rhombic species. The optimized fit is in trace c. Although the overall shape appears to be qualitatively correct, the intensities are consistently wrong at the g_z of the second species and also at the trough of the g_y feature of the second species.

Further progress required a change of paradigm: what was assumed to be a g_y of a second species (i.e., a derivative-shaped feature) is really a g_z of a third species (i.e., an absorption-shaped feature). In general, all the features on the low-field side of the main perpendicular feature in this and all other HiPIP spectra (see later) can only be fitted assuming that they are all different g_zs. This implies that all spectra consist of three or more components.

The next step was to keep the parameters of the major rhombic component approximately constant and to add two additional components initially assuming axial symmetry. From the fit, trace d, it is concluded that yet one more component must be present. Also a poor fit of the positive/negative intensity of the major perpendicular region persists. The latter was cured by making the first two minor components rhombic with g-strain anisotropy comparable to that of the main component. Then, the third minor component was added and optimized. After a final global optimization, the resulting trace e was obtained with the parameters shown in Table 1. Of course, the overlap in the perpendicular region is considerable, therefore not all the parameters of each individual component were determined. However, a major conclusion can be drawn that the EPR spectrum of *A. vinosum* HiPIP requires a minimum of *four*

separate components to be fitted. The sums of the squared residuals as a percentage of that for the final fit are 806, 255, 248, 152, and 100% for traces a–e, respectively.

Systematic inventory of HiPIP EPR

The EPR spectra of seven HiPIPs from six microbial sources were analyzed. The final results are compiled in Table 2 and are shown in Fig. 3. Two HiPIPs have a minor spectral component that is suspect since its g values differ significantly from all other sets found: *E. vacuolata* isoprotein I ($g_x = 2.01$) and *R. gelatinosus* ($g_x = 1.98$). These minor components are possibly from breakdown products.

For some fits a significant noncollinearity of the g strain was required. None of the spectra have the complexity of the *A. vinosum* wild-type HiPIP EPR; however, all fits are indicative of at least *three* different components. It appears that the current literature model of HiPIPs as constituted of different valence isomers [2, 7–9] is consistent with the EPR; it must include more than two isomers to account for the complexity found in the g-strained EPR from the $[4Fe–4S]^{3+}$ cluster of any of the seven different HiPIP proteins.

Comparison with previous studies

In an early Mössbauer study on the $[4Fe–4S]^{3+}$ cluster of *A. vinosum* HiPIP, Dickson et al. [22] found two opposing hyperfine fields in the spectra taken with an applied magnetic field and at a temperature of 4 K, which suggested an inequivalence in the iron ions. The electron–nuclear double resonance measurements by Anderson et al. [23] led to a similar conclusion. In a subsequent attempt at quantitative Mössbauer spectroscopy, in 1980, Middleton et al. [4] decided to fit their data under the model of two independent components in a one-to-one stoichiometry. This key assumption implies two types of iron ions grouped as pairs, which translates to the reasonable physical picture of an Fe^{3+}–Fe^{3+} pair and an Fe^{3+}–Fe^{2+} pair with delocalization of the extra electron over the mixed-valence pair, and with parallel magnetic coupling between irons within a pair and antiparallel coupling between the pairs, resulting in the observed system spin $S = 1/2$.

Antanaitis and Moss [11] were the first, in 1975, to use frequency-dependent EPR for the study of HiPIP. The data on *A. vinosum* HiPIP taken at 9 and 35 GHz indicated that the peak positions correspond to real g values and that broadening is dominated by g strain, although these conclusions were not drawn at that time. Spectral simulation of signal multiplicity suggested two major and one minor species, which is qualitatively and quantitatively inconsistent with the present analysis. It was later reported by Dunham et al. [18] that *A. vinosum* HiPIP dimerizes upon freezing in high-salt solution (a typical condition to store HiPIPs), which results in dipolar interaction. Moulis et al. [12] studied the selenium derivative of *A. vinosum* HiPIP, i.e., containing a $[4Fe–4Se]^{3+}$ cluster. Simulation of the spectrum required four rhombic species with respective weights of 65, 18, 10, and 7%. This result is somewhat closer to ours for the native protein (Table 2); however, this simulation was not based on a rationalized broadening model. The same ad hoc simulation approach was more recently applied to the EPR of *H. halophila* HiPIP I [6], and the result (one major and only one minor component) is qualitatively similar to ours (three components, cf. Table 2).

Gloux et al. [9] and Le Pape et al. [10] studied synthetic model compounds containing the $[Fe_4S_4]^{3+}$ core using single-crystal EPR. The dilute $[Fe_4S_4]^{3+}$ centers were created by γ-irradiation of crystallized $[Fe_4S_4]^{2+}$ core containing compounds. Site multiplicity was clearly detected and this provided the first instance of a straightforward interpretation of EPR data in terms of different topologies for the mixed-valence pair. Interestingly, five different species were identified for a symmetrical model compound and three different species for an asymmetrical model compound, which appears to be broadly consistent with the contention that in a fully symmetrical $[4Fe–4S]^{3+}$ cluster each of the six possible topologies for the mixed-valence pair should be equally likely. Single-crystal EPR has the distinct advantage that knowledge of the complex angular dependence of the line width is not required for the analysis of a single-orientation spectrum. Unfortunately, sensitivity problems have thus far precluded single-crystal EPR studies on HiPIP proteins.

Gloux et al. [9] also discussed the EPR spectrum of *A. vinosum* HiPIP, and, with reference to unpublished experiments by J. Gaillard, they reached the conclusion that the spectrum is made up of four different components. The interpretation was partially based on different saturation behavior of spectral features. We would like to point out that the theory of g strain implies continuously varying saturation behavior over the powder envelope of a *single* species [20]; therefore, differential saturation is *not* a reliable criterion for deconvolution of these complex spectra.

In one case only thus far has it been possible to quantitatively super-reduce a HiPIP to the $[4Fe–4S]^{1+}$ state: Heering et al. [24] super-reduced *R. globiformis* HiPIP with Ti(III)citrate. The resulting EPR spectrum shows a multiplicity of components, and this indicates that the occurrence of valence isomers in biological [4Fe–4S] clusters is not limited to the 3+ state. Also, the $[Fe_4S_4]^{1+}$ core in γ-irradiated model compounds occurs in more than one form [9].

Relation to average paramagnetic NMR shifts

Bertini et al. [7, 8, 25–27] showed that the model of a single, localized mixed-valence pair was insufficient to

explain the complex pattern of temperature-dependent paramagnetic shifts in the resonances from βCH_2 protons in HiPIP. They proposed a minimum model with two topologies for the mixed-valence pair, which was parameterized in terms of the percentage ferric character of a particular iron ion of the cluster (Cys-36 bound Fe in *H. halophila* HiPIP I [8]). A plot of averaged hyperfine shift of, e.g., the βCH_2 protons of Cys-36 versus the percentage ferric character was found to be approximately linear. The point of calibration was the shift data from *H. halophila* HiPIP II. Its $[4Fe–4S]^{3+}$ cluster accidentally exists as a single-valence isomer on the basis of EPR [28] and NMR data [8, 29].

It is at present not possible to assign a specific EPR subspectrum to a specific geometrical valence isomer. Therefore, it is not obvious how the NMR and EPR data can be compared quantitatively. In the quoted NMR analysis, the percentage ferric character of Cys-36 bound Fe runs from 24% (*H. halophila* I) to 70% (*R. gelatinosus*). The EPR intensities reported in Table 2 cannot be grouped in a set that would be quantitatively consistent with the percentage ferric character deduced from NMR. This inconsistency may well reflect different valence isomer distributions at cryogenic (EPR) and ambient (NMR) temperatures. Indeed, inspection of the fractional intensities of the various isomers at low temperature suggests that, at variance with room temperature estimates, one isomer is always largely predominant over the others.

Nevertheless, a qualitative correlation is indicated. The isomer having the mixed-valence pair on the irons bound to cysteines II and III (counting system defined in Ref. [8]), and assumed to be the only one present in the HiPIP II from *H. halophila*, could be the one with the highest g_z feature ($g_z = 2.145$). According to the NMR data, the relative amount of this isomer decreases in the following order: *H. halophila* II > *H. halophila* I > *R. globiformis* > *E. vacuolata* I > *E. vacuolata* II > *A. vinosum* > *R. gelatinosus*. In the EPR spectra, the isomer with the highest g_z value decreases in a similar order, *H. halophila* II > *H. halophila* I > *R. globiformis* > *E. vacuolata* II > *E. vacuolata* I ≈ *A. vinosum*, and is absent in *R. gelatinosus*. For the isomer with the mixed-valence pair bound to cysteines III and IV [8], the correlation is less obvious, but this could correspond to the EPR isomer, which is dominant in *E. vacuolata* I and *E. vacuolata* II, *R. gelatinosus*, and *R. tenuis*. This isomer would be characterized by a g_z value of 2.103–2.113.

Concluding remarks

The present work describes quantitative resolution of one major and several minor components in the EPR of several HiPIPs. With reference to previous magnetic spectroscopy studies it is proposed that these components can be reasonably assigned to valence isomers of the cubane.

The biological relevance of multiple valence isomers has not been established. The main biological functions of HiPIPs appear to be electron transfer between membrane-bound respiratory-chain complexes of photosynthetic bacteria ([30] and references quoted therein), and charge transport for DNA repair ([31] and references quoted therein). Valence isomers are not commonly found in $[4Fe–4S]^{1+}$ ferredoxins. The redox active molecular orbitals of ferredoxins and HiPIPs appear to differ considerably in their ligand character [32]. It is possible that valence isomer multiplicity of HiPIPs is related to the high-potential redox chemistry of the proteins. To our knowledge, no experimental data (e.g., EPR line shape analysis as a function of redox potential) are available yet to test such a hypothesis.

References

1. Sands RH, Dunham WR (1974) Quart Rev Biophys 7:443–504
2. Bertini I, Ciurli S, Luchinat C (1995) Struct Bonding 83:1–54
3. Papaefthymiou V, Girerd J-J, Moura I, Moura JJG, Münck E (1987) J Am Chem Soc 109:4703–4710
4. Middleton P, Dickson DPE, Johnson CE, Rush JD (1980) Eur J Biochem 104:289–296
5. Bertini I, Campos AP, Luchinat C, Teixeira M (1993) J Inorg Biochem 52:227–234
6. Dilg AWE, Mincione G, Achterhold K, Iakovleva O, Mentler M, Luchinat C, Bertini I, Parak FG (1999) J Biol Inorg Chem 4:727–741
7. Banci L, Bertini I, Ciurli S, Ferretti S, Luchinat C, Piccioli M (1993) Biochemistry 32:9387–9397
8. Bertini I, Capozzi F, Eltis LD, Felli IC, Luchinat C, Piccioli M (1995) Inorg Chem 34:2516–2523
9. Gloux J, Gloux P, Lamotte B, Mouesca J-M, Rius G (1994) J Am Chem Soc 116:1953–1961
10. le Pape L, Lamotte B, Mouesca JM, Rius G (1997) J Am Chem Soc 119:9757–9770
11. Antanaitis BC, Moss TH (1975) Biochim Biophys Acta 405:262–279
12. Moulis J-M, Lutz M, Gailliard J, Noodleman L (1988) Biochemistry 27:8712–8719
13. Hagen WR, Hearshen DO, Sands RH, Dunham WR (1985) J Magn Reson 61:220–232
14. Hagen WR, Hearshen DO, Harding LJ, Dunham WR (1985) J Magn Reson 61:233–244
15. Hagen WR (1989) In: Hoff AJ (ed) Advanced EPR; Applications in biology and biochemistry. Elsevier, Amsterdam, pp 785–812
16. Heering HA, Bulsink YBM, Hagen WR, Meyer TE (1995) Biochemistry 34:14675–14686
17. van Dam PJ, Klaassen AAK, Reijerse EJ, Hagen WR (1997) J Magn Reson 130:140–144
18. Dunham WR, Hagen WR, Fee JA, Sands RH, Dunbar JB, Humblet C (1991) Biochim Biophys Acta 1079:253–262
19. Hearshen DO, Hagen WR, Sands RH, Grande HJ, Crespi HL, Gunsalus IC, Dunham WR (1986) J Magn Reson 69:440–459
20. Hagen WR, Albracht SPJ (1982) Biochim Biophys Acta 702:61–71
21. Savitzky A, Golay MJE (1964) Anal Chem 36:1627–1639
22. Dickson DPE, Johnson CE, Cammack R, Evans MCW, Hall DO, Rao KK (1974) Biochem J 139:105–108
23. Anderson RE, Anger G, Petersson L, Ehrenberg A, Cammack R, Hall DO, Mullinger R, Rao KK (1975) Biochim Biophys Acta 376:63–71

24. Heering HA, Bulsink YBM, Hagen WR, Meyer TE (1995) Eur J Biochem 232:811–817
25. Bertini I, Briganti F, Luchinat C, Scozzafava A, Sola M (1991) J Am Chem Soc 113:1237–1245
26. Bertini I, Capozzi F, Ciurli S, Luchinat C, Messori L, Piccioli M (1992) J Am Chem Soc 114:3332–3340
27. Bertini I, Capozzi F, Luchinat C (2003) ACS Symposium Series 858:272–286
28. Kappl R, Ciurli S, Luchinat C, Hüttermann J (1999) J Am Chem Soc 121:1925–1935
29. Banci L, Bertini I, Capozzi F, Carloni P, Ciurli S, Luchinat C, Piccioli M (1993) J Am Chem Soc 115:3431–3440
30. Meyer TE, Cusanovich MA (2003) Photosynthesis Res 76:111–126
31. Boon EM, Livingston AL, Chmiel NH, David SS, Barton JK (2003) Proc Natl Acad Sci USA 100:12543–12547
32. Dey A, Glaser T, Couture MM-J, Eltis LD, Holm RH, Hedman B, Hodgson KO, Solomon EI (2004) J Am Chem Soc 126:8320—8328